

# **Efficiency of IllustrisTNG in simulating galaxy properties**

Comparing the output of the IllustrisTNG simulation to observational data.

**Aurora Grefsrud**

Project report



Institute of Physics  
NTNU  
Norway  
November 18, 2020

# Abstract

## Contents

<b>1</b>	<b>Introduction</b>	<b>2</b>
1.1	Motivation . . . . .	2
1.2	The structure of this report . . . . .	3
<b>2</b>	<b>Theory</b>	<b>3</b>
2.1	Galaxy formation . . . . .	4
2.1.1	Dark matter halos . . . . .	5
2.1.2	Galaxies . . . . .	6
2.1.3	Stellar-to-Halo mass relation . . . . .	7
2.2	Galaxy evolution and classification . . . . .	8
2.2.1	Elliptical (early type) galaxies . . . . .	10
2.2.2	Spiral (late type) galaxies . . . . .	10
2.3	Galaxy properties . . . . .	12
2.3.1	The Tully-Fisher relation . . . . .	12
2.3.2	The Faber-Jackson relation and the Fundamental Plane	14
2.3.3	Color bimodality . . . . .	15
2.3.4	Supermassive Black Holes . . . . .	15
<b>3</b>	<b>Method</b>	<b>16</b>
3.1	IllustrisTNG . . . . .	16
3.1.1	The simulations . . . . .	16
3.1.2	Data catalogues . . . . .	17
3.1.3	Selection criteria . . . . .	19
3.2	Observational data . . . . .	20
3.2.1	SAMI Galaxy Survey . . . . .	20
3.2.2	Other data sets . . . . .	20
3.3	Calculating properties . . . . .	21
3.3.1	Cosmologies and property value representation . . . . .	21
3.3.2	Separating out early and late type galaxies . . . . .	22
3.3.3	Circular velocities . . . . .	23
3.3.4	Effective radius . . . . .	23
<b>4</b>	<b>Results and discussions</b>	<b>24</b>
4.1	SHMR . . . . .	24

4.2	TFR . . . . .	24
4.3	FJ relation and the FP . . . . .	27
4.4	Color bimodality . . . . .	27
4.5	SMBH relations . . . . .	34
<b>5</b>	<b>Conclusions</b>	<b>35</b>

# 1 Introduction

## 1.1 Motivation

The field of astrophysics is a relatively young field of study compared to most other disciplines of science, but in many ways it is also the most fundamental. From the tiniest quantum fluctuations at the beginning of time, to galaxy clusters, astrophysicists have to cover a range of magnitudes from the smallest particles discovered to the largest structures in the universe.

In this project galaxies are the focus of study. Theories for how galaxies formed and evolved since the Big Bang have been proposed since they were first discovered, and as new data and new physics emerge, new theories take over for old ones. The model that has been established as the one currently best able to explain observations of the universe is the Lambda cold dark matter ( $\Lambda$ CDM) model. In this model, the energy in the universe is made up of about 75 percent dark energy (the so-called vacuum energy that is pushing the expansion of the Universe), 21 percent dark matter and about 4 percent baryonic (visible) matter (Mo, Bosch, et al. 2010a).

There are many theories for what dark matter actually is (see e.g. Boveia et al. 2018), but what we do know is that cosmological models require the presence of dark matter to reproduce the structures seen today. Dark matter does not interact with any particles except through gravity. In the  $\Lambda$ CDM model of our universe, galaxies are located in the center of dark matter halos (hereafter, halos), which extend much further than the actual visible galaxy. Many of the properties of galaxies are linked to its host halo. These, along with several other galaxy properties, are the main focus of this project report.

Hydrodynamical cosmological simulations have been around since the 1980s, starting as N-body simulations of only dark matter particles with a set of

initial conditions (Frenk et al. 1983). As computers became more powerful, and physicists learned more about the complicated physics of galaxies, the simulations started to incorporate stars, gas and other baryonic components. The resolution and size of simulations have increased tremendously. Now it is possible to have mass resolutions that show the inner structure of galaxies and at the same time have a simulation volume that is large enough to be relevant on cosmological scales. In this respect, projects such as the Illustris, Millenium and EAGLE simulations have pushed the boundaries of modern astrophysics. IllustrisTNG is the new and improved version of the Illustris simulation. The first result-papers were published in 2017, and more data is being produced still. It increases the resolution, size and amounts of physics included, to produce the largest, most detailed simulated universe to this date.

In this report, the data from the IllustrisTNG simulations will be compared against observational data, to determine whether it manages to reproduce known galaxy properties. The data used is from the readily available data catalogues, and so this will also be a good way to check the usefulness of this resource.

## 1.2 The structure of this report

In this report I aim to give a thorough and in-depth explanation of my work during the fall semester of 2020. Section 2 explains the physics of the main galaxy property relations that are covered in this report. It also hopefully serves as a sort of glossary and explanation for many of the, sometimes confusing, astrophysical terms. In section 3, I explain how the simulation and observation data is filtered and converted to the right units for comparison. Section 4 covers the actual comparison of the data, while the section 5 sums up what was learned from the project and looks to the future for what should be studied next.

## 2 Theory

Some astrophysics terms and constants:

- $z$  - Redshift, a dimensionless measure of time where  $z = 0$  denotes the current time and  $z \rightarrow \infty$  as we move back in time towards the

beginning of the universe. The redshift also gives the actual physical frequency shift of light emitted from a source moving away from us in an expanding universe.

- $H_0$  - The Hubble constant is a cosmological constant related to the expansion rate of the universe. The best measurements of today set the value of  $H_0$  to 67.8 km/s/Mpc. Specifically, this means that a galaxy located 100 Mpc from us is receding from us at a velocity of 67.8 km/s because of the expansion of the universe.
- $h$  - The “little hubble constant” is given by  $H_0 = 100 h$  km/s/Mpc, and often appears in astrophysics data as a representation of the uncertainty of the Hubble constant. See section 3.3.1 for further discussion on this.
- $G$  - gravitational constant
- $M_*$  - stellar mass
- $M_\odot$  - solar mass. In astrophysics, masses are always given in units of solar masses.
- $L$  - luminosity. The luminosity is the ..  
//Will add more here as I see the need.

## 2.1 Galaxy formation

Our understanding of the formation and evolution of the universe as a whole is based on the cosmological principle, which states that matter is distributed spatially isotropically and homogeneously across the universe on large scales. Of course, we would not have any structure formation if the matter was actually perfectly uniformly distributed in the very beginning of the universe. It is not completely clear how this initial deviation from homogeneity originated, but at very early times after the Big Bang, the universe was so small that quantum effects would have played a significant role. These tiny quantum fluctuations may then have been responsible for the initial structure formation we can observe today.

Given that these initial density fluctuations in matter were present, gravitational effects will then amplify the overdense regions of space as matter is pulled together. If the universe did not expand, these instabilities in the

density field would just keep growing. However, we know the universe is expanding, and so the effect is dampened significantly. As matter keeps being pulled in over time, the overdense region might reach a “turn-around size” where the gravitational pull is large enough to compensate for the expansion rate of space. Then the matter will collapse towards the center. The exact process for collapse is beyond the scope of this report, but it depends on the ratio of dark matter to baryonic matter, and the properties of the dark matter itself.

### 2.1.1 Dark matter halos

Dark matter halos are the result of such initial overdense regions of dark matter particles. Halos cover a huge range in magnitudes of mass lower than  $10^9 M_\odot$  up to sizes of at least  $10^{15} M_\odot$ . In general, halos are ellipsoid in shape. The spherically averaged density profile of halos, as predicted by N-body simulations of dark matter in a  $\Lambda$ CDM universe, is well described by the Frank-Nevarro-White profile (Navarro et al. 1996),

$$\frac{\rho}{\rho_{crit}} = \frac{\delta_c}{(r/r_s)(1+r/r_s)^2}. \quad (1)$$

$\rho_{crit} = 3H_0^2/8\pi G$  is the critical density,  $\delta_c$  is the characteristic overdensity and  $r_s$  is the scale radius. Both  $\delta_c$  and  $r_s$  may vary for each halo.

Halos grow hierarchically through mergers of smaller halos into larger halos. A smaller halo that merges with a larger halo may survive as a separate entity within the host halo and is then known as a subhalo.

One of the most interesting properties of a  $\Lambda$ CDM universe is the halo mass function, the number density of halos as a function of their mass. In a famous paper by William H. Press and Paul Schechter (Press et al. 1974), the halo mass function is defined as:

$$\frac{dn}{dM} = f(\sigma) \frac{\bar{\rho}}{M^2} \frac{d\log(\sigma^{-1})}{d\log(M)}. \quad (2)$$

Where  $\sigma(R)$  is the variance of the field with a smoothing radius R,  $\bar{\rho}$  is the mean density of the universe and  $f(\sigma)$  is the multiplicity function. For that

paper,  $f(\sigma)$  was found to be

$$f(\sigma) = \frac{2}{\pi} \sigma \exp(-\sigma^2/2), \quad (3)$$

but other models will give a different multiplicity function. //add figure

We will not cover the mathematical details of this analytical solution to the mass function, but it is based on the assumption of spherical collapse, and is not dependent on cosmology or redshift. Until the end of the century, numerical simulations tended to agree with the 1974 results. However, newer and more complex numerical solutions have shown that the Press-Schechter formalism tends to overestimate the amount of smaller halos, while under-predicting the abundance of larger halos. There has also been several studies that show how the mass function actually is slightly redshift-dependent (e.g. Tinker et al. 2008).

### 2.1.2 Galaxies

As dark matter halos formed in the very early universe, they created a gravitational potential well which gave room for the primordial baryonic matter (ionized hydrogen gas) to start collapsing. As the density of the gas increased, temperature increased and halted the collapse, but through several radiation cooling processes the gas was able to collapse enough for fusion to start and stars to be born. Because of the halos role as initial potential wells, the baryonic matter collapsed in such a way that it formed a spinning disk around the center of the halo. This was the birth of galaxies as we know them today.

Galaxies are mainly composed of stars and hot gas, with a smaller contribution of stellar remnants, cold gas and dust. Hot gas is hydrogen gas that is fully ionized, and does not collapse into stars, while cold gas has a much lower temperature and can contribute to star formation. There are at least two trillion galaxies in the observable universe (Conselice et al. 2016), with stellar masses ranging from  $< 10^6 M_\odot$  to  $10^{12} M_\odot$ .

It has been found that a large fraction of the galaxies are gravitationally bound to each other in groups and clusters. Galaxy clusters are the largest gravitationally bound systems in the Universe, and can span a distance of several megaparsecs. They typically contain more than a hundred galaxies,

as well as large amounts of intergalactic gas. Galaxies in galaxy clusters serve an important purpose to astrophysicists, as they essentially function as tracers of the largest halos in the universe.

The  $\Lambda$ CDM model for our universe gives a bottom-up solution to galaxy formation, a hierarchical formation. Essentially this means that larger galaxies have formed through mergers of smaller galaxies. When a galaxy forms, the angular momentum of its initial components get transferred to the galaxy as a whole, and the result is a rotating disk galaxy. Galaxies that are not pure disk galaxies, but have an elliptical component of stars and gas with pressure dominated random motions and which extends in all directions from the center, are results of the merging of galaxies. As many galaxies exist in clusters, the likelihood of a galaxy merger is higher than one might otherwise expect in those regions, and so galaxy clusters contain more elliptical galaxies.

A very important property of the galaxy population is the galaxy luminosity function, which gives the number density of galaxies as a function of their luminosity. The luminosity of a galaxy is directly proportional to its stellar mass, so the luminosity function also gives us the mass distribution of galaxies. Mathematically, the luminosity function is defined as  $\phi(L)dL$ , the number density of galaxies in the luminosity range  $L \pm dL/2$ . In 1976 Paul Schechter proposed a fit to the luminosity function of galaxies on the form

$$\phi(L)dL = \phi^*(L/L^*)^\alpha \exp(-L/L^*)dL/L^*, \quad (4)$$

//add figure

where  $\phi^*$  is a normalization,  $L^*$  is the characteristic luminosity for that sample of galaxies (it will differ for instance for galaxies within a cluster compared to isolated galaxies) and  $\alpha$  is the slope of the power law where  $L \ll L^*$  (Schechter 1976). This Schechter function is still a good fit to this day, and is in excellent agreement for galaxies with  $L \gg L^*$ . For the low mass range of galaxies, the parameter  $\alpha$  must be found, and this is one of the challenges of astrophysicists that study galaxy properties.

### 2.1.3 Stellar-to-Halo mass relation

The stellar-to-halo mass relation (SHMR) is a relation which gives the stellar mass of a galaxy as a function of its host halo mass. This is particularly

difficult to find empirically, as it is not possible to directly measure the dark matter halo mass.

One way of looking for this relation is through a method called abundance matching. In abundance matching, the numerically found halo mass function and the observationally found luminosity function are combined. This is done using the simple assumption that the largest halo contains the largest galaxy, the second largest halo contains the second largest halo and so on. By mapping each galaxy to its corresponding halo in such a fashion, the shape of the SHMR can be found directly.

Using abundance matching, the SHMR has been found to be well described by a power law with different slopes for the low-mass and high-mass end of the spectrum (Behroozi et al. 2013).

//add figure

Other ways of studying the SHMR is through simulations which include both the halo mass and the corresponding stellar mass for that halo, or through inferring the halo mass by using the rotational curves of disk galaxies (see section 2.2.2).

## 2.2 Galaxy evolution and classification

As soon as telescopes became good enough to clearly make out galaxies in the sky, it became apparent to astronomers that galaxies come in many different shapes and sizes. The morphology of a galaxy is important because it turns out that morphology is closely linked to other properties of the galaxy. Edwin Hubble classified galaxies on a spectra (Hubble 1926), with elliptical galaxies (galaxies that have a dominant spheroidal component) on one end of the spectrum and spiral galaxies (galaxies with a prominent disk component) on the other (see Figure 1). As the galaxy types were presented as a sequence, Hubble deemed it convenient to use the adjectives “early” and “late” to describe the two extreme ends of the spectrum. He did consider the fact that these words might be confusing because of their temporal connotations, but went ahead with using “early” and “late” as a proxy for “less complex” and “more complex”, respectively. Indeed this turned out to be confusing, as it is now established that galaxies actually evolve with time along the sequence, starting out as late-type disk galaxies and often ending up as more massive early-type ellipticals.

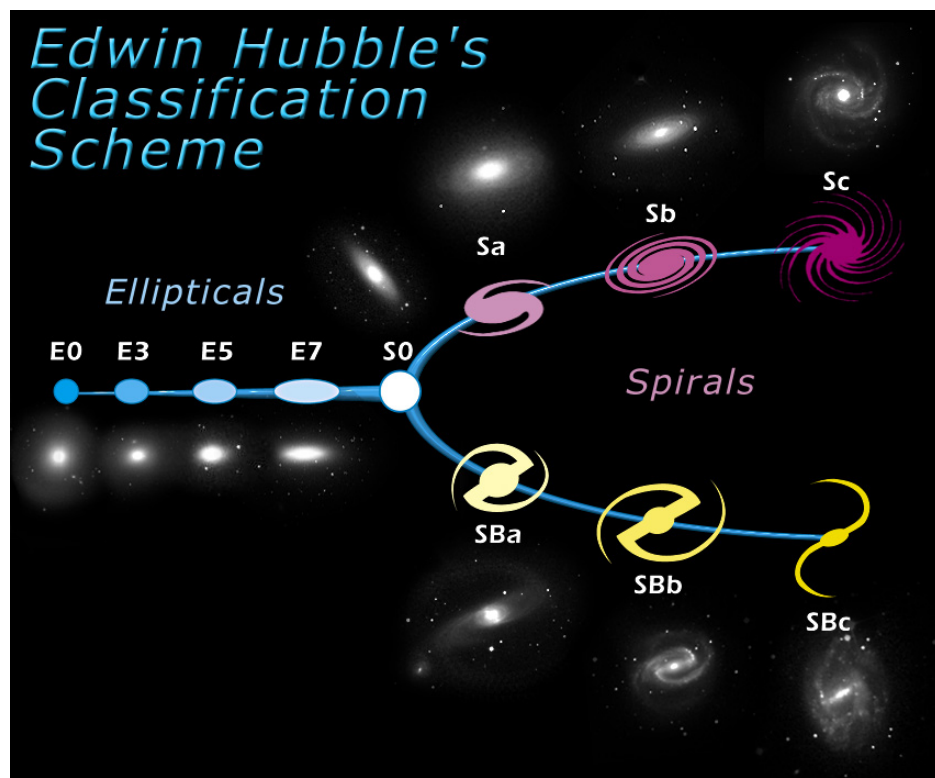


Figure 1: Chart from 1999 showing the original classifications of galaxy morphology. Credit: ESA/Hubble

In the  $\Lambda$ CDM model, galaxies grow through mergers. Mergers are separated into two types, major and minor mergers. Major mergers are events where two galaxies of equal size collide and become one galaxy. Simulations have shown that a major merger between two disk galaxies produces an elliptical. The Milky Way, which is a large spiral galaxy ( $M_* > 10^{10}$ ) has probably grown through many smaller minor mergers, and thus kept its disky part.

It is not always easy to distinguish between a disky elliptical and a spiral with a large spheroidal component (bulge). Some galaxies are also in the middle of a merging process. These can have very irregular shapes, and so are hard to classify. Other galaxies are very small, so called dwarf galaxies. These galaxies tend to have very little stellar mass compared to dark matter, so they do not exhibit the properties of ellipticals, even though they may be more elliptical in shape.

### 2.2.1 Elliptical (early type) galaxies

Elliptical galaxies are mainly pressure-dominated systems, meaning that the motion of the stars is predominantly radial. The largest galaxies in the universe tend to be ellipticals, but they come in all sizes. The star population of ellipticals is generally older than that of spirals, and there is usually little to no star formation. There is very little gas and dust in ellipticals, and they tend to emit more light in the redder end of the EM spectrum. Early type galaxies are less common than late type galaxies, and are more usually found in galaxy clusters.

### 2.2.2 Spiral (late type) galaxies

Late type galaxies have a prominent disky component, orbiting around the galaxy's center. The rotational velocity of the disk is typically much larger than the velocity dispersion of the galaxy's bulge. The stars in a spiral galaxy are usually much younger than those in early types. There is a lot of gas and dust present in spirals, giving rise to ongoing star formation. Late type galaxies are bluer in color than early types. Field galaxies, galaxies that are not part of a galaxy cluster, are predominantly spirals.

The rotational velocities of the stars at different radii in the disk of spiral galaxies can be measured observationally, and plotting the velocity as a function of radius gives us the velocity curve of the galaxy. If the mass in the

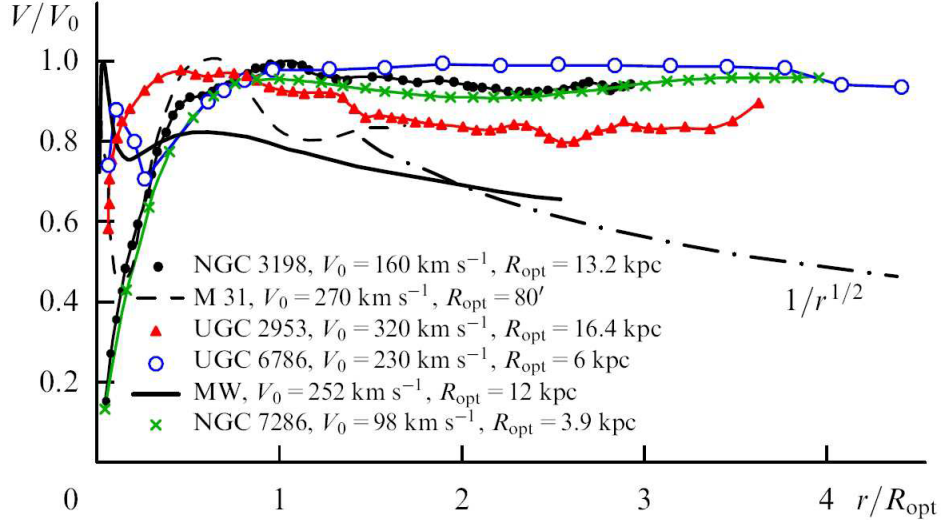


Figure 2: Rotation curves for several spiral galaxies. The dashed line is the expected curve if there was no dark matter. Credit: Zasov et al. 2017.

galaxy was solely made up of the gas and stars that we are able to detect optically, we would expect the velocity curve to drop off as we get to the outer parts of the galaxy. Assuming the particles move in circular orbits around the center of mass, the circular velocity at a given radius is given by the formula

$$v_{circ} = \sqrt{GM(< R)/R}, \quad (5)$$

where  $M(< R)$  is the total mass inside the radius  $R$ . However, the observational data shows that the velocity curve does not fall off towards the outer parts of the galaxy, but actually flattens out (see Figure 2). This perplexed early astrophysicists, as the mass inside the outer radius must be much greater than that which could be accounted for by the stars and gas in the galaxy. An effort to solve this problem led to the theory of dark matter, and later to the  $\Lambda$ CDM model.

The main differences between early and late-type galaxies is summed up in table 1.

	Early type	Late type
Shape	Spheroidal	Disk
Color	Red	Blue
Velocity direction	radial	circular
Stellar population	older	younger
Star formation rate	low	high
Size	smaller	larger
Gas and dust	little	much

Table 1: Galaxy properties by morphology type

## 2.3 Galaxy properties

### 2.3.1 The Tully-Fisher relation

In 1977, R.B. Tully and J.R. Fisher (Tully et al. 1977) published a paper where they found a surprisingly good correlation between the luminosity of a spiral galaxy and the characteristic rotational speed of its disk on the form of a simple power law with index  $\alpha$ ,

$$L \propto v_{rot}^\alpha, \quad (6)$$

as seen in Figure 3. This is known as the Tully-Fisher relation (TFR). As stellar mass is directly proportional to the luminosity, this gives us the ability to estimate stellar mass from a simple measurement of the rotational velocity.

$$M_* \propto v_{rot}^\alpha \quad (7)$$

$\alpha$  was found to be 3.7. Later work has found  $\alpha$  to lie between 3.5 and 4 (needs citing...).

This relation is a great tool for estimating the distance to a galaxy, as the calculated luminosity can be compared to the observed luminosity at Earth. For numerical simulations, being able to reproduce the TFR is an essential way to check if the model used is reliable.

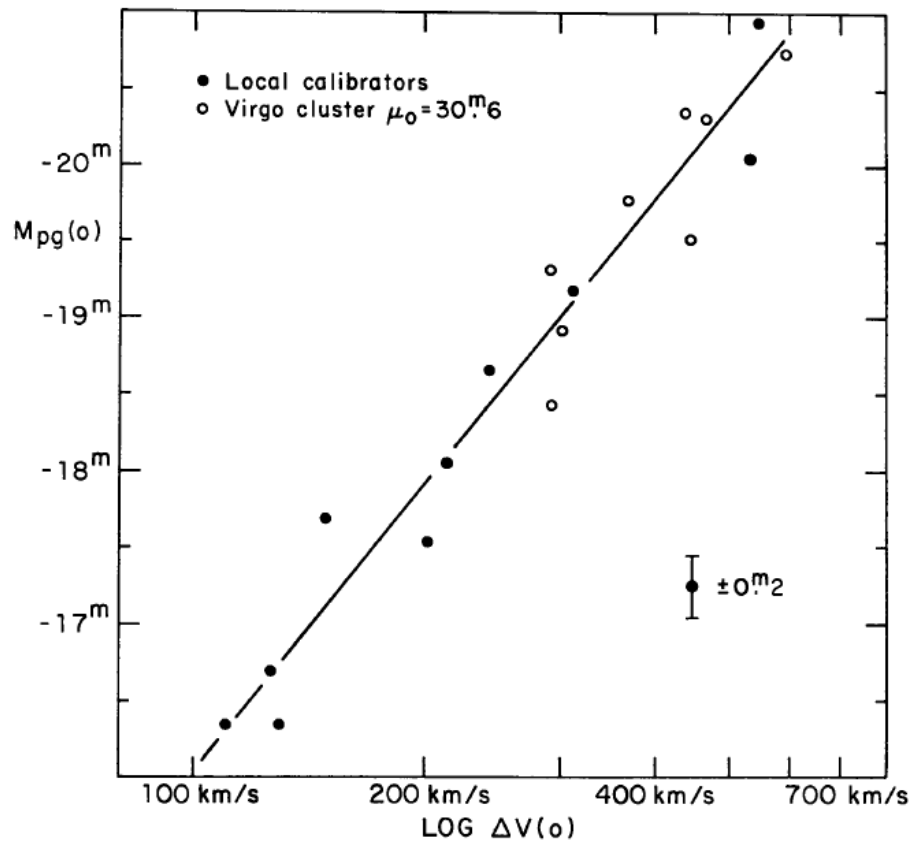


Figure 3: The original figure from the 1977 paper by R.B. Tully and J.R. Fisher, showing the linear fit for the luminosity - velocity values in the log-log plane. Credit: Tully et al. 1977

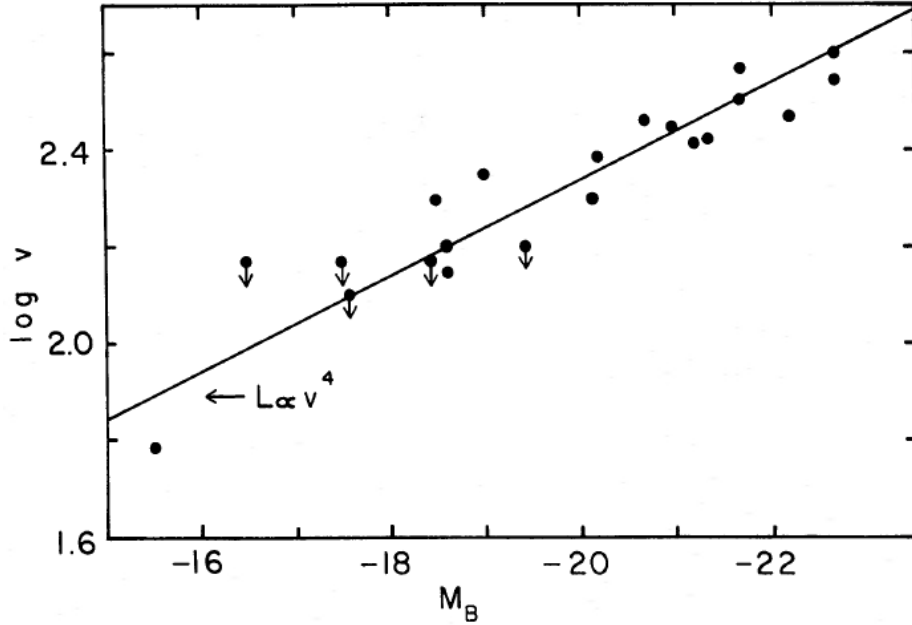


Figure 4: The original fit for the Faber-Jackson relation as presented in the 1976 paper. It shows the velocity dispersion as function of the luminosity in the log-log plane, along with a power law with index 4. Credit: Faber et al. 1976

### 2.3.2 The Faber-Jackson relation and the Fundamental Plane

At around the same time that Tully and Fisher published their paper, Sandra M. Faber and Robert Earl Jackson published a paper that linked the velocity dispersion and luminosity of early-type galaxies. The proposed relation was on the form of a power law as well,

$$L \propto \sigma^\gamma, \quad (8)$$

with a power law index  $\gamma$  of approximately 4 (Faber et al. 1976). Their results are shown in Figure 4.

This is known as the Faber-Jackson (FJ) relation. The scatter in the FJ relation was larger than that found for the TFR however, and it was later found that the velocity dispersion also was dependent on the size of the

galaxy.

$$\sigma \propto L^a R^b \quad (9)$$

With the radius added into the equation, the scatter became much less significant. Most ellipticals are found on the same plane in  $\sigma, R, L$  space. This plane became known as the Fundamental Plane (FP), through a paper published in 1987 (Djorgovski et al. 1987), and is also something which successful numerical simulations must reproduce.

//Add FP figure

### 2.3.3 Color bimodality

Color, in astrophysics, is defined as the difference in magnitudes measured for a galaxy by two different optical filters. A galaxy that is "blue" has a larger amount of blue light than red. In general, galaxies are found to inhabit one of two groups on a color-mass diagram, blue and red (see Figure 5). The blue galaxies are most often smaller late type galaxies, while the red ones are mainly larger early types. There are many factors that contribute to the color of a galaxy, like stellar age and metallicity as well as the amount of gas the light has passed through and its metallicity.

//five ugriz SDSS broadband filters

### 2.3.4 Supermassive Black Holes

Almost every large galaxy with a spheroidal component has a supermassive black hole (SMBH) in its center. These are black holes with masses over  $10^6 M_\odot$  and even above  $10^9 M_\odot$ . The mass of the SMBH correlates surprisingly well with other properties of the galaxy, such as the velocity dispersion and luminosity. This is surprising because the SMBH only has a gravitational influence within a very small radius compared to the entire galaxy, which suggests that the SMBH evolves along with the galaxy and that their formation is linked. In fact, it seems very likely that these gigantic black holes play a vital role in galaxy evolution, and are a central component of the galaxy as a whole.

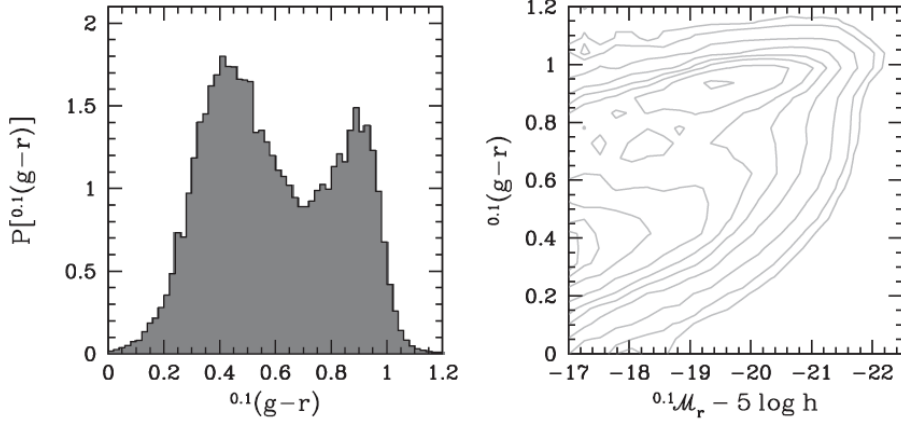


Figure 5: To the left: The probability density of colors of over 350 000 galaxies in the Sloan Digital Sky Survey. To the right: The color-magnitude relation for the same galaxies, clearly showing two distinct populations. Credit: Mo, van den Bosch, et al. 2010b

### 3 Method

#### 3.1 IllustrisTNG

IllustrisTNG<sup>1</sup> is the follow-up project after the success of the Illustris simulations. It is a huge project, built upon a magneto-hydrodynamical cosmological simulation code with added physical processes on a subgrid level (Weinberger et al. 2016). Adding physical processes like gas radiation, star formation, stellar feedback through supernova explosions, supermassive blackhole accretion and magnetic fields are essential to model galaxy formation and evolution, and allows a much better comparison to reality. The data output from the simulations is extensive, and is not meant to be analysed all in one go, but rather through a series of analyses, each targeting a specific scientific question.

##### 3.1.1 The simulations

The IllustrisTNG project includes 18 different simulations with varying resolutions, spatial size and included physics. There are three main simulations

---

<sup>1</sup><https://www.tng-project.org/>

	Volume [ $Mpc^3$ ]	$N_{DM}$	$m_{DM} [M_\odot]$	$m_{baryon} [M_\odot]$
TNG50	$51.7^3$	$2163^3$	$4.5 \times 10^5$	$8.5 \times 10^4$
TNG100	$110.7^3$	$1820^3$	$7.5 \times 10^6$	$1.4 \times 10^6$
TNG300	$302.6^3$	$2500^3$	$5.9 \times 10^7$	$1.1 \times 10^7$

Table 2: The simulation details for the three main TNG simulations.  $N_{DM}$  is the amount of dark matter particles.  $m_{DM}$  and  $m_{baryon}$  is the mass of the dark matter and baryonic particles, respectively.

that differ in volume and resolution, and the details of these are summed up in Table 2. Each of the main simulations have been run at three different resolution levels, which makes it possible to study how changing only the resolution in a given simulation affects the outcome. TNG100 has a physical box volume of  $110.7^3 Mpc^3$ , and a baryonic particle resolution of  $1.4 \times 10^6 M_\odot$ , while the TNG300 simulation has a volume of  $302.6^3 Mpc^3$  and a baryonic particle resolution of  $1.1 \times 10^7 M_\odot$ . The TNG50 data is actually not yet available, but it is expected soon, and provides a much higher resolution in a smaller box size. In this project, a large statistical sample of galaxies was needed, as well as detailed structure of the inner part of the galaxies to calculate the different properties, so the TNG100 simulation was the ideal middle ground with respect to size and resolution. The TNG100-1 simulation data has been used throughout the project, which is the highest available resolution for TNG100, and will from now on be references as "TNG" only. A visual representation of parts of the simulations can be seen in Figure 6. TNG uses the results from the Planck Collaboration for its cosmology parameters,  $\Omega_{\Lambda,0} = 0.6911$ ,  $\Omega_{m,0} = 0.3089$ ,  $\Omega_{b,0} = 0.0486$ ,  $\sigma_8 = 0.8159$ ,  $n_s = 0.9667$  and  $h = 0.6774$  (Ade et al. 2016). See section 3.3.1 for more details.

### 3.1.2 Data catalogues

All the Illustris-TNG data is publically available online at the TNG webpage. The data products that are available for each simulation are snapshots, group catalogs and merger trees as well as some supplementary data sets. There are 100 snapshots for each run, which are taken at specific redshifts. They include all the particles in the whole volume of the simulation, with 20 of them including all the particle fields for each particle as well. There are five different particle types, and each particle has its properties stored as particle fields. These fields include information like position, kinematic data and

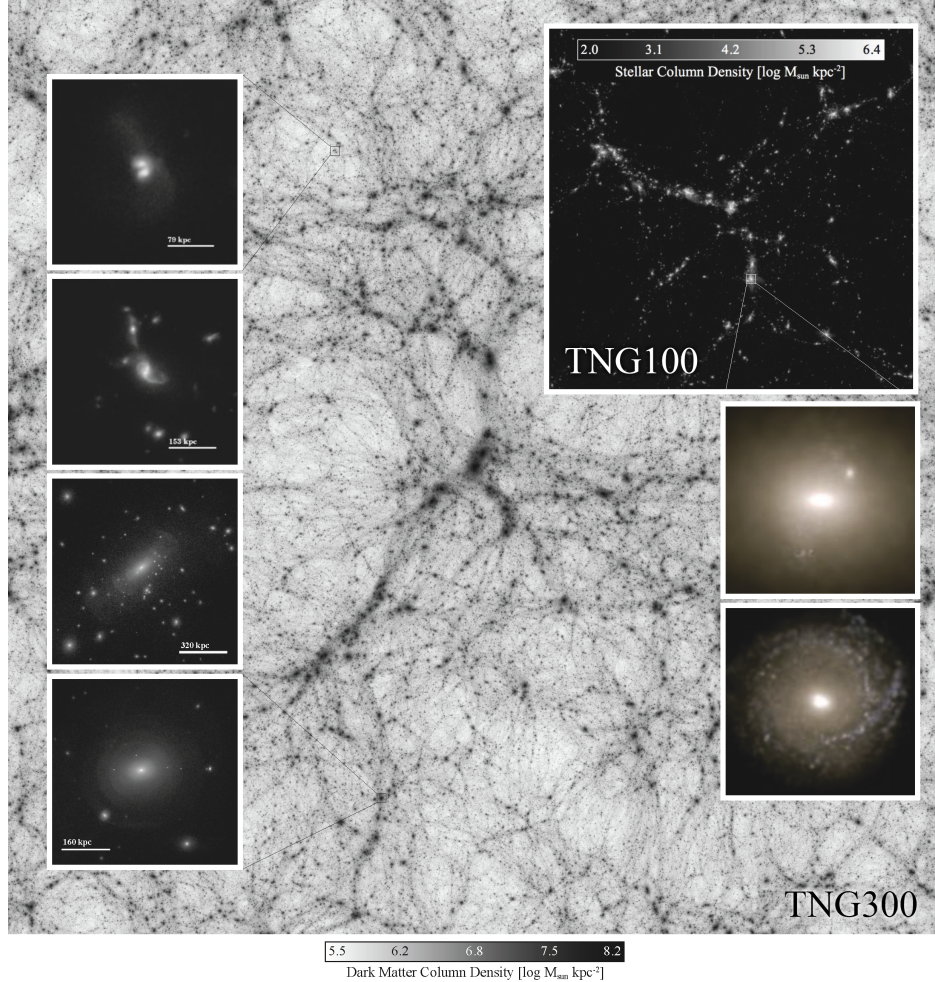


Figure 6: A composite image that illustrates the two simulations TNG100 and TNG300. In the background is the dark matter distribution for the whole TNG300 volume. In the upper right is the stellar mass distribution across the entire TNG100 volume. The panels on the left show galaxy-galaxy interactions, while the panels on the right show the stellar light projections of two  $z = 0$  galaxies. Credit: TNG Collaboration

atomic/chemical composition.

The group catalogs provide a convenient way to quickly access already calculated properties of the different halos and subhalos instead of dealing with all the particles in a snapshot. This saves a lot of time and effort, but gives the user less control over what can be analysed. In future work, it might be interesting to do the calculations directly from the snapshots myself. There is one group catalog for each snapshot, and this includes two types of objects, Friends-of-Friends (FoF) and Subfind. The FoF catalog contains all the halos, and the Subfind catalog contains all the subhalos for each halo. Each subhalo has a parent halo, and the largest subhalo in each halo is the central subhalo. The merger trees data products contain the merger history of each subhalo.

This project makes use of the group catalogs for the  $z = 0$  snapshot in TNG100-1, as we want to compare the output data to observations of the local (present time) universe.

### 3.1.3 Selection criteria

The TNG documentation recommends filtering out all subhalos that are flagged with the *SubhaloFlag* field, and so these were cut from the data. These are most probably subhalos of non-cosmological origin, and so should not be considered real galaxies.

For most of the relations covered in this project, it is desirable to only use the central galaxies in each halo. This is because satellite galaxies are more affected by their environment, which in turn affects the kinematic and structural properties of the galaxy. This will naturally lead to a scatter in the galaxy scaling relations that are being studied, which central galaxies will not display. The FoF catalog contains the index for the largest subhalo in each halo, so combining this information with the Subfind catalog allows one to create a subset of the data that contains only the central galaxies.

Only galaxies with stellar mass greater than  $10^9 M_\odot$  are used, except for the SHMR analysis, where galaxies with stellar mass down to  $10^8 M_\odot$  are included. This is because smaller galaxies will have fewer stellar particles, and thus their structure is not necessarily reliably resolved.

## 3.2 Observational data

//Some general introduction to observational data goes here

It is desirable to use the same observational data when comparing different scaling relations, however it has not been possible to do that. This is because we are analysing such different problems as stellar-to-halo mass and SMBH relations, which require very different kind of measurements. A compromise has been to use one main survey for the kinematic scaling relations.

//fill in when you know more about this //

### 3.2.1 SAMI Galaxy Survey

The Sydney – Australian Astronomical Observatory Multi-Object Integral Field Spectrograph (SAMI) is mounted on the Anglo-Saxon telescope in Australia. The SAMI Galaxy Survey<sup>2</sup> is a spectroscopic survey of a large sample of galaxies in the nearby universe ( $z < 0.113$ ). The survey was started in 2013, and ended in 2018. There have been two major data releases, with the newest being Data Release Two (DR2) (Scott et al. 2018). DR2 includes data for 1559 galaxies, which is about 50 % of the full galaxy survey. The data products available are IFS data cubes and 2D maps, as well as catalogue data. Analysing data cubes and 2D maps falls outside the scope of this product, so catalogue data is used where possible.

Rotational velocities were not available as catalogue data, but in Bloom et al. 2017 the calculations were already done, and the best fit for the TFR was used in our comparison:  $\log(V_{rot}) = 0.31 \pm 0.0092 \times \log(M_*) - 0.93 \pm 0.1$ .

### 3.2.2 Other data sets

For the SHMR best fit models from two different abundance method papers were used in the comparison to TNG.

In Moster et al. 2012 a double power law was used to fit the data,

$$M_*/M_{halo} = 2N[(\frac{M}{M_1})^{-\beta} + (\frac{M}{M_1})^\gamma]^{-1}, \quad (10)$$

---

<sup>2</sup><https://sami-survey.org/>

where  $N$  is a normalization parameter,  $M_1$  is a characteristic mass and  $\beta, \gamma$  are the slopes at the low and high-mass end respectively. The best fit for the four free parameters at redshift  $z = 0$  are given as  $M_1 = 11.590 \pm 0.236$ ,  $N = 0.0351 \pm 0.0058$ ,  $\beta = 1.376 \pm 0.153$  and  $\gamma = 0.608 \pm 0.059$ .

Behroozi et al. 2013 improved the fit by using a power law for the high mass end, and a subpower law for the low mass end.

$$\log(M_*(M_h)) = \log(\epsilon M_1) + f(\log(M_h/M_1)) - f(0), \quad (11)$$

$$f(x) = -\log(10^{\alpha x} + 1) + \delta \frac{(\log(1 + \exp(x)))^\gamma}{1 + \exp(10^{-x})}$$

Here  $M_1$  is a characteristic halo mass,  $\delta$  is the strength of the subpower law,  $\alpha$  is the power law slope for  $M_h \ll M_1$  and  $\gamma$  is the power law index for  $M_h \gg M_1$ . The values for the parameters are  $M_1 = 11.514 \pm (0.053, 0.009)$ ,  $\delta = 3.508 \pm (0.087, -0.369)$ ,  $\alpha = -1.412 \pm (0.020, -0.105)$ ,  $\epsilon = -1.777 \pm (0.133, 0.146)$  and  $\gamma = 0.316 \pm (0.076, -0.012)$ .

The more recent work by Zanisi et al. 2019 was also used, which employed the same function for the fit as Behroozi et al., but with other values for the parameters. This study chose to only use central galaxies from the Sloan Digital Sky Survey (SDSS). The parameters were found to be  $M_1 = 11.632 \pm (0.008, 0.009)$ ,  $\delta = 3.797 \pm (0.026, 0.021)$ ,  $\alpha = -2.352 \pm (0.026, -0.021)$ ,  $\epsilon = -1.785 \pm (0.010, 0.008)$  and  $\gamma = 0.600 \pm (0.10, 0.013)$ .

//Tundo and Ferrarese

### 3.3 Calculating properties

#### 3.3.1 Cosmologies and property value representation

When making measurements of galaxy properties at cosmological distances, some assumptions about the underlying cosmology of the universe must be made. One of these assumptions is the value of the Hubble constant  $H_0$ , more commonly represented by  $h$ . This constant is also used when properties are calculated using a simulation. For IllustrisTNG,  $H_0 = 100 h$  km/s/Mpc with  $h = 0.6774$  and the explicit  $h$ -dependence of each property value is stated clearly in the documentation. For the SAMI data catalogue, no  $h$ -dependence is explicitly stated in the documentation or data release papers,

	$M_*$	$M_{halo}$	$R_e$	Luminosity	Velocity
TNG	$M_\odot h^{-1}$	$M_\odot h^{-1}$	$\text{kpc } h^{-1}$	mag	km/s
Observations	$M_\odot h^{-2}$	$M_\odot h^{-1}$	$\text{kpc } h^{-1}$	mag +5 log( $h$ )	km/s

Table 3: ...

but the Hubble constant used is given,  $h = 0.7$ . Behroozi et al. 2013 uses  $h = 0.7$  as well. In Moster et al. 2012 a value of  $h = 0.704$  is chosen. For the BHMR papers, Ferrarese et al. 2000 does not state which cosmology is used and seems to use a mix of distance measurements, while Tundo et al. 2007 uses  $h = 0.7$ .

Best practice dictates that conversion between different cosmology-parameters should be done by replacing the  $h$  with the most recent value for  $h$  and evaluating the values which can then be compared (Croton 2013). In Table 3 the  $h$ -dependence of the properties of TNG as well as the common  $h$ -dependences for observational data is shown along with the corresponding units. //add more here about what I ended up doing//

IllustrisTNG-distances are given as comoving distances. For  $z = 0$ , the proper and comoving distance of two objects are the same so no conversion is needed.

//add information about IMF here //

### 3.3.2 Separating out early and late type galaxies

As several of the relations studied in this project relate to the morphological type of the galaxies, it is interesting to filter out early and late type galaxies to study separately. This can be done in different ways, and in many studies of TNG several criteria for classification have been chosen. In this case, the fraction of gas inside the effective radius of each galaxy has been chosen as the single criteria for classification. Including a criteria for star formation rate did not significantly change the outcome, so it was determined to keep the selection process simple.

$$M_{gas}/M = f \quad (12)$$

For  $f > 0.1$ , the galaxy is classified as late type, while for  $f < 0.1$ , the galaxy

is classified as early type.

In the SAMI DR2, the galaxy morphology is determined visually. They are classified into four different categories: ellipticals, S0, Sa/Sb and Sc/Sd/irregulars. See Figure 1 in section 2.2 for a visualisation of the different galaxy classifications.

### 3.3.3 Circular velocities

To compare the simulation data with observational data for rotational velocities, calculated circular velocities are used. The Subhalo field `SubhaloVMax` gives the maximum value for the spherically averaged rotation curve. As the rotational curves are nearly flat for large enough radii, it is not very important at which radius the observational rotational velocity is measured, as long as it is in the flat part of the curve.

For the SAMI-data velocity curves were only available as 2D maps and not catalog data. An analysis of the TFR for the SAMI Galaxy Survey had already been done in Bloom et al. 2017, so the best fit from that paper was used to represent the observational rotational velocities. They chose the rotational velocity at  $2.2 R_e$ , which should lay well into the flat regime of the velocity curve, and coincide well with the maximum velocity.

### 3.3.4 Effective radius

In observational data, galaxy sizes are always projected sizes, as they are derived from 2D pictures. A common measure of the size of a galaxy is the effective radius, which is the radius within which half the light of the galaxy is contained. This quantity depends on the analysis and quality of the 2D profiles, and may not be able to include all the light in a galaxy in the way that we can ensure for computer simulated data. The radius also depends on which band the measurements are made in, as different bands will capture different parts of the galaxy.

For TNG data, the `SubhaloHalfmassRadStellar` field has been used. The half-mass radius is the radius of a spherical volume within which half the stellar mass is found. This can be considered as the 3D half-mass radius, as it is not a projected quantity. This value is generally higher than the 2D projected half-light radius for a given mass up to  $M_* < 10^{10.5}$ , as seen in (Genel et al. 2017).

The SAMI catalog data takes the values for the effective radius from the GAMA Sérsic catalogue (Kelvin et al. 2012). The effective radius is defined as the semi-major axis half-light radius, measured in the r-band. The values are given in units of arcseconds. The `astropy` python package was used to convert these to a comoving distance in kpc.

To convert the elliptical radius to circular radius, the definition of ellipticity  $\epsilon$  is used:

$$r_{e,circ} = r_{e,sm} \sqrt{(1 - \epsilon)}, \quad (13)$$

where  $r_{e,circ}$  is the circular radius and  $r_{e,sm}$  is the semi-major axis effective radius.

## 4 Results and discussions

### 4.1 SHMR

The SHMR for all the galaxies, as well as only the central galaxies, with  $M_* > 10^8 M_\odot$  from TNG is plotted in figure 7, along with the best fits from Moster et al. 2012, Behroozi et al. 2013 and Zanisi et al. 2019. When calculating the SHMR using all the galaxies, the median values are pushed towards lower halo masses compared to only central galaxies. As mentioned earlier, the central galaxies are less affected by environmental conditions, and so they better reflect the “isolated galaxy evolution”. Compared to the data, the central galaxy SHMR falls right in between the fits from Moster et al. and Behroozi et al. for lower mass galaxies. However, the steepness of the slope is closer to that of Zainsi et al. Above the characteristic halo mass of  $\approx 10^{11.6} M_\odot$ , the TNG SHMR deviates significantly from the abundance matching fit by having a much steeper slope. This indicates a value for  $\gamma$  in equation 11 closer to unity. The more recent, centrals only, results from Zanisi et al. agrees better with the high mass slope than the other two, but the difference is still significant.

### 4.2 TFR

The TFR for the late type galaxies in TNG is shown in Figure 8 along with the best fit for the SAMI data found in Bloom et al. 2017. The slope of the

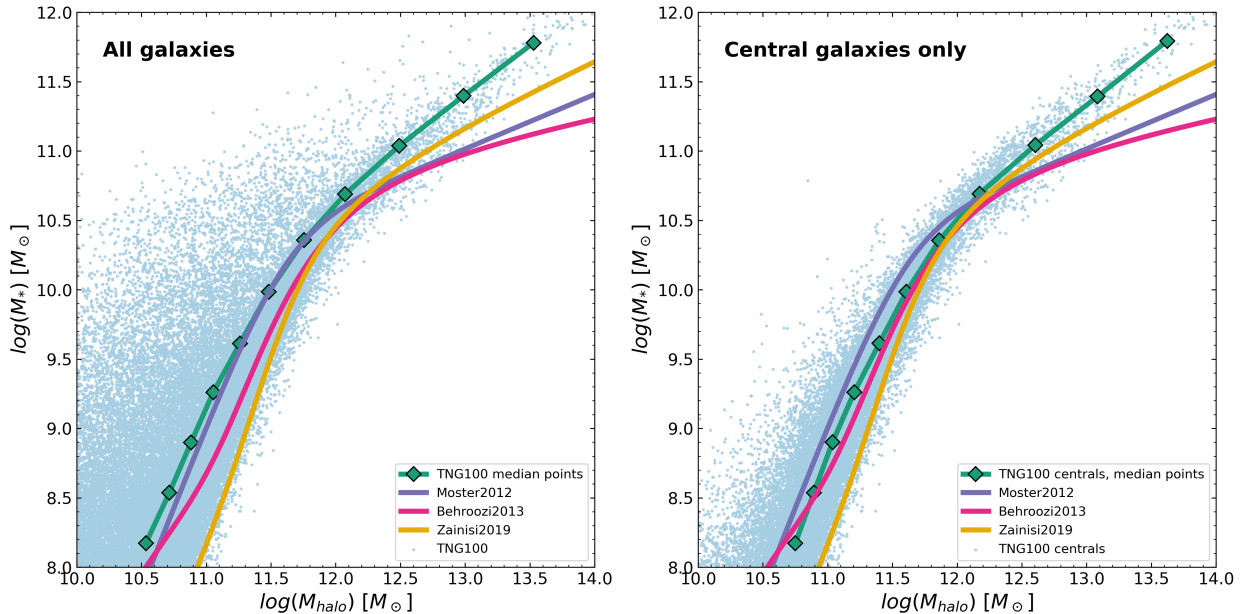


Figure 7: The SHMR of the TNG simulation for all galaxies above stellar mass  $10^8 M_\odot$ . The best fit from abundance matching from three different papers (Moster et al. 2012, Behroozi et al. 2013 and Zanisi et al. 2019) are also shown.

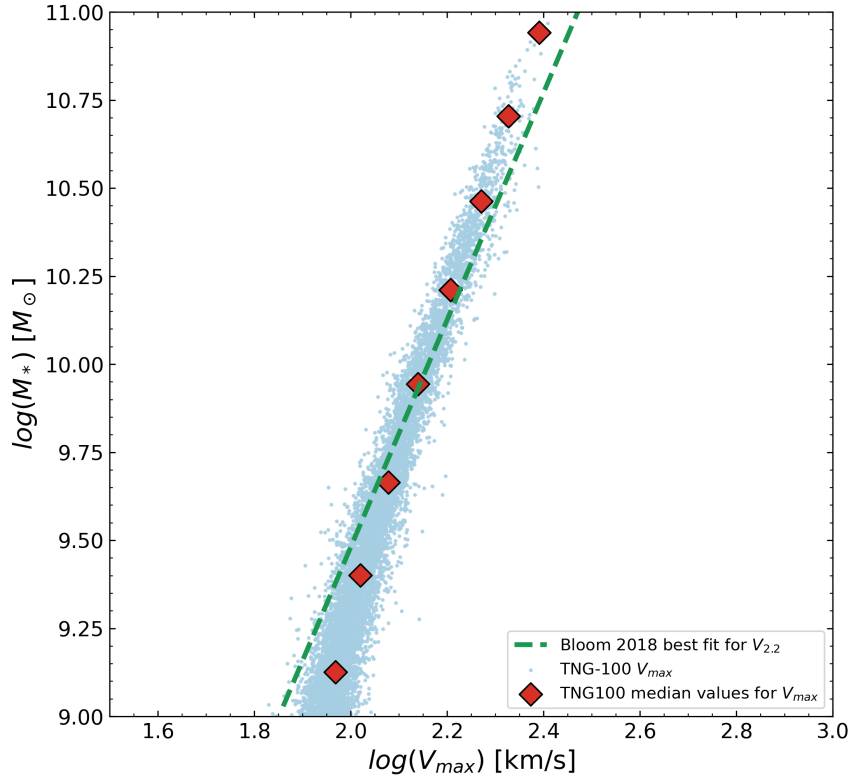


Figure 8

TNG TFR seems to be slightly steeper than for Bloom et al. 2017. Rotational velocities for TNG are chosen as the maximum velocity in the velocity curve, while Bloom et al. use the velocity at  $r = 2.2r_e$ . This could lead to the velocity measurements of the smaller galaxies being systematically lower for Bloom et al. compared to TNG. A better comparison would be to choose the same definition for the rotational velocity for both data sets. Also, it might be interesting to investigate the Baryonic Tully-Fisher relation by adding the HI-mass and velocity measurements to the stellar measurements.

### 4.3 FJ relation and the FP

The velocity dispersion as function of stellar mass can be seen in Figure 9. The trend for the TNG-100 data is a clear power law as expected from the FJ relation. Compared to the observational data, the simulation data shows lower  $\sigma$  values, by about 0.1-0.2 dex. This could be explained by the fact that the  $\sigma$  in the TNG galaxies is averaged across all particles, across the whole size of the subhalo. In general, gas has a lower  $\sigma$  than stars and dark matter, so this could push the total  $\sigma$  down. However, in early-type galaxies there is little gas so the impact would be expected to be small. The fact that  $\sigma$  is found by averaging across the entire subhalo would include particles further out than for the SAMI data in which the velocity dispersion is averaged inside the effective radius ( $\sigma_e$ ) is used. Other studies have also found that simulations tend to get lower values for  $\sigma$  (Sande et al. 2018), so this might also just be a limitation of the simulations.

The other relations in the fundamental plane are shown in Figures 10 and 10. The mass-radius relation for TNG is in excellent agreement with SAMI for larger galaxies. For galaxies with  $M_* < 10^9 M_\odot$ , there are so few data points for SAMI that the comparison is not really meaningful.

The  $\sigma$ -radius relation is also affected by the systematically lower  $\sigma$  values for TNG.

### 4.4 Color bimodality

The color-mass diagrams for different filters are shown in Figure 12. There is a distinct separation between early and late type galaxies, as expected. The distinction is clear in all bandfilters.

Figure 13 shows the probability density function (PDF) for TNG100 early and late type galaxies for different filters. The separation into two main density peaks is apparent in all filters. In Figure 14 the PDF for the TNG100 (g-i) band and the SAMI (g-i) band are shown. The peaks coincide well for the two data sets, although the distribution in galaxies is different. This is likely because TNG has a larger amount of smaller, late-type blue galaxies, which are much more difficult to observe than larger and generally redder galaxies. A mass weighted PDF might give a more fair comparison.

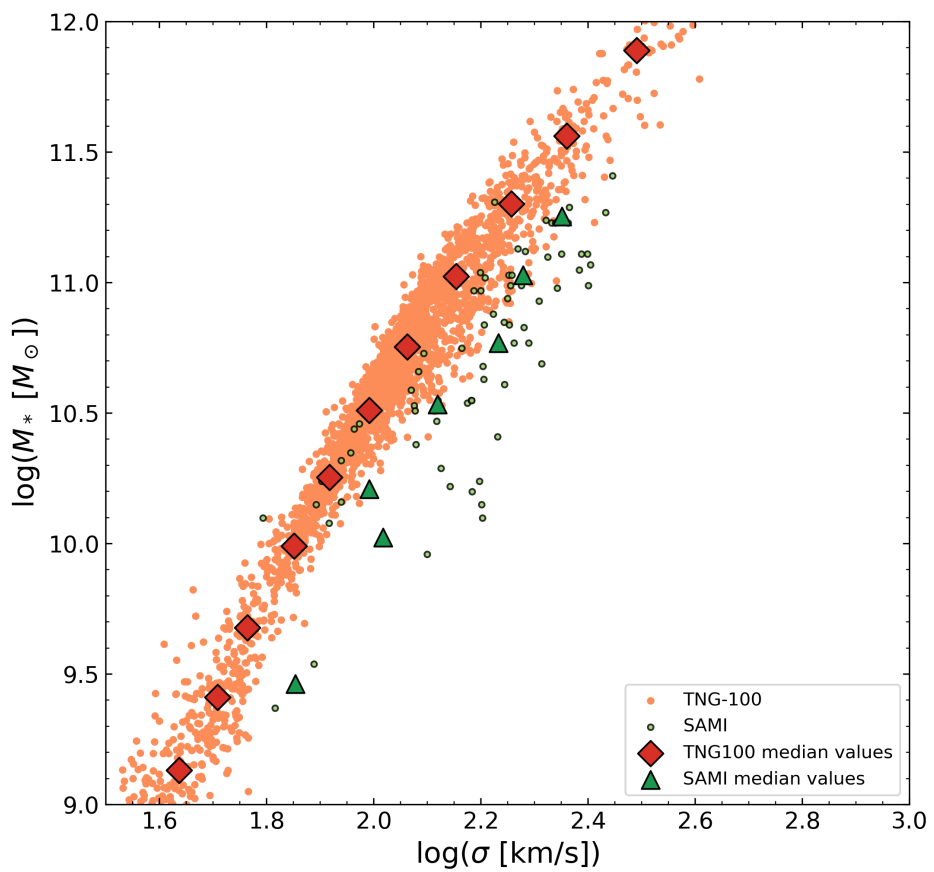


Figure 9: Early type galaxies for both TNG and SAMI.

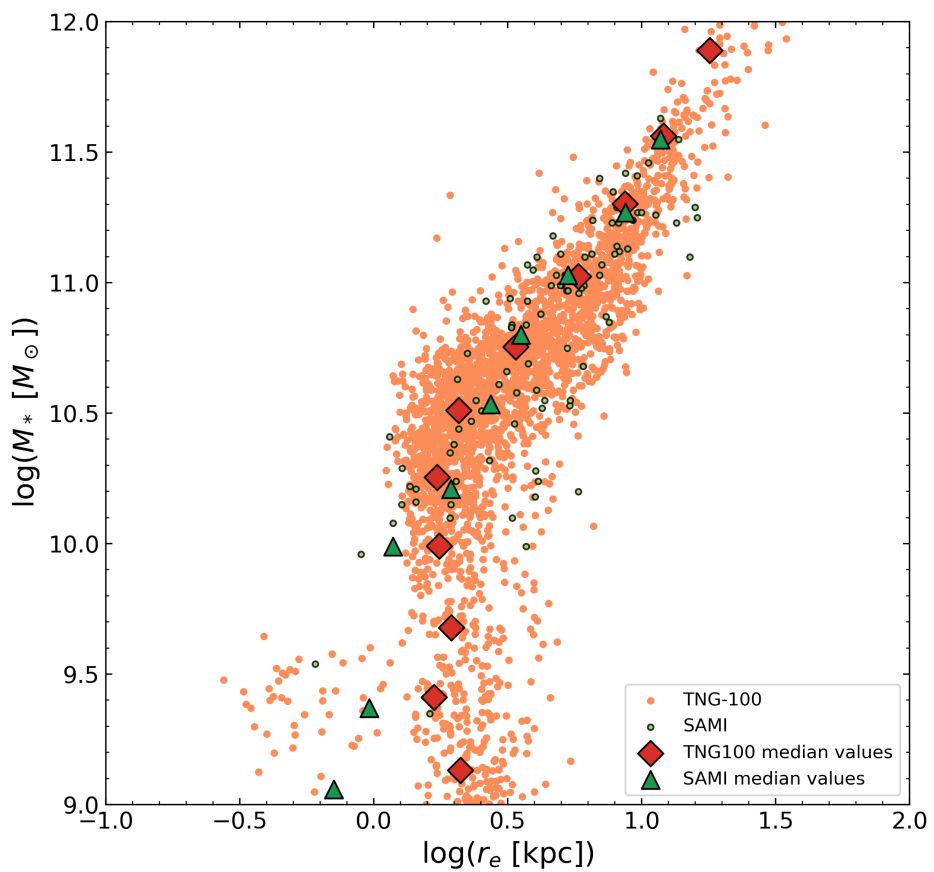


Figure 10: Early type galaxies for both TNG and SAMI.

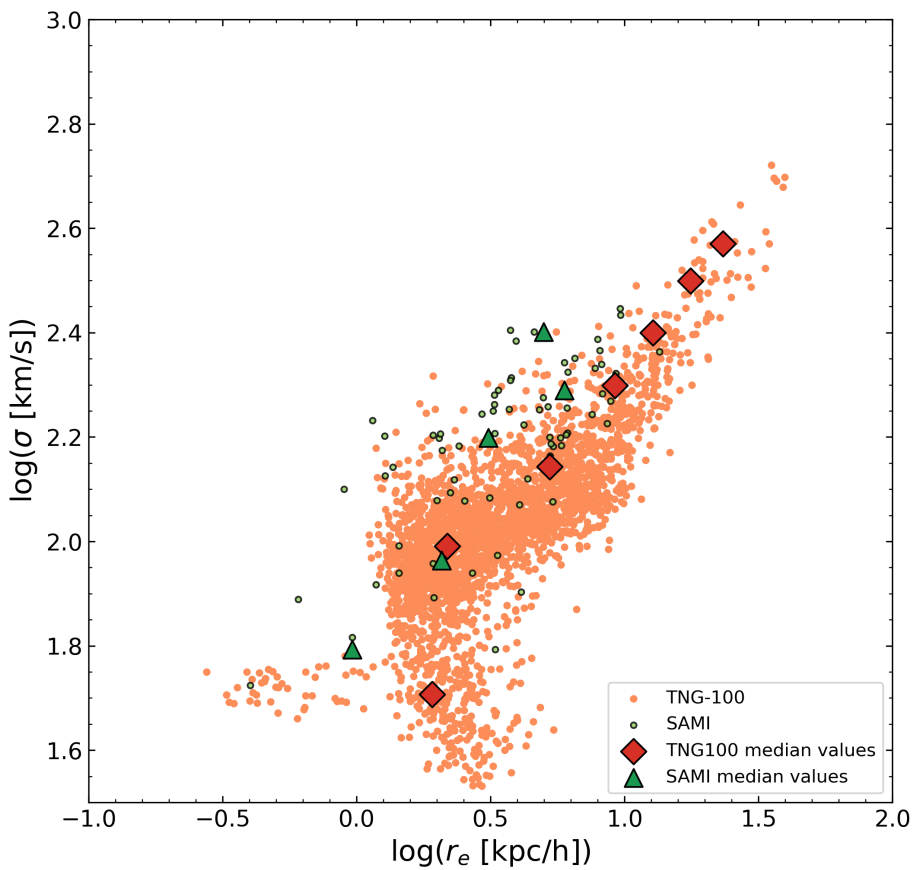


Figure 11: Early type galaxies for both TNG and SAMI.

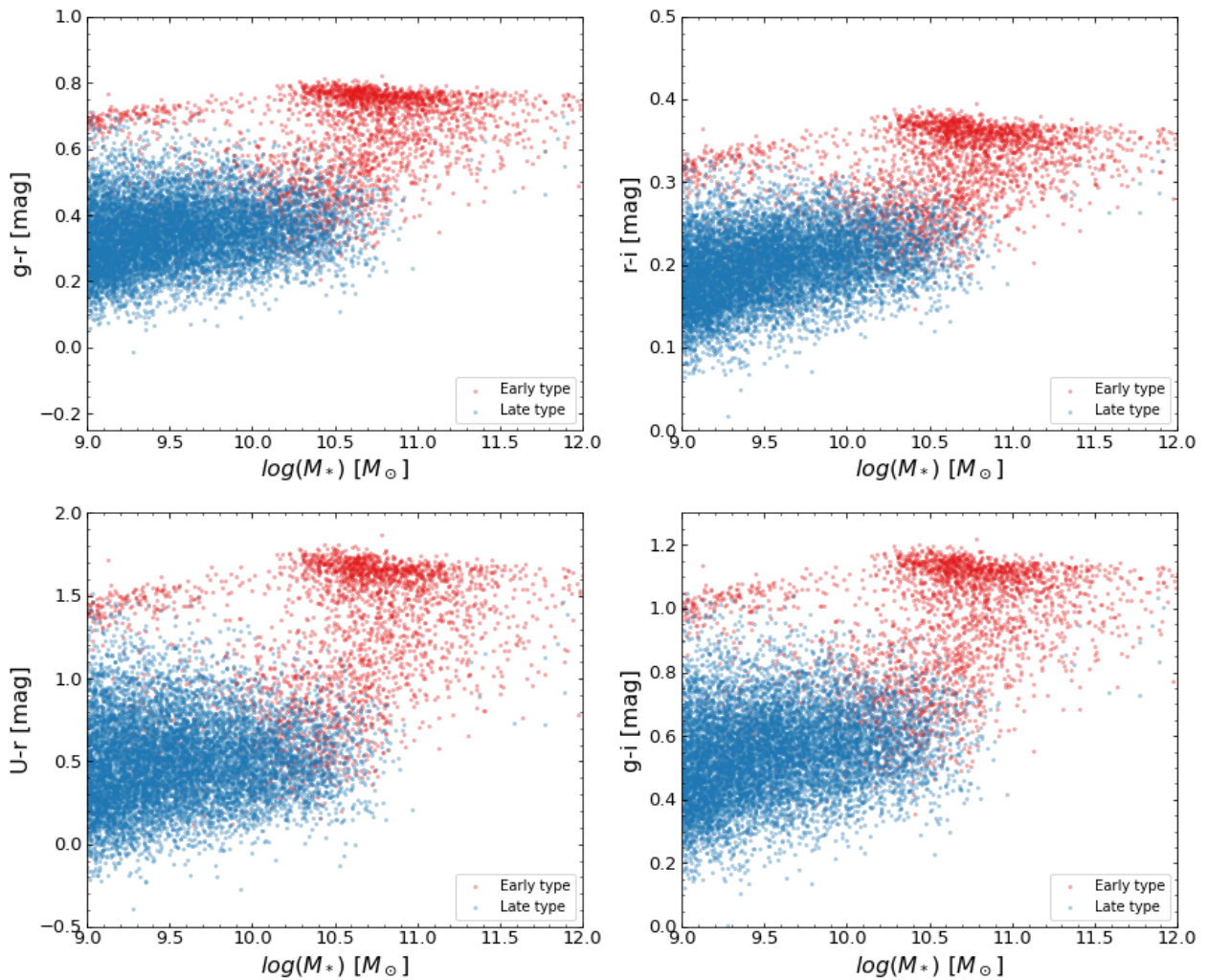


Figure 12

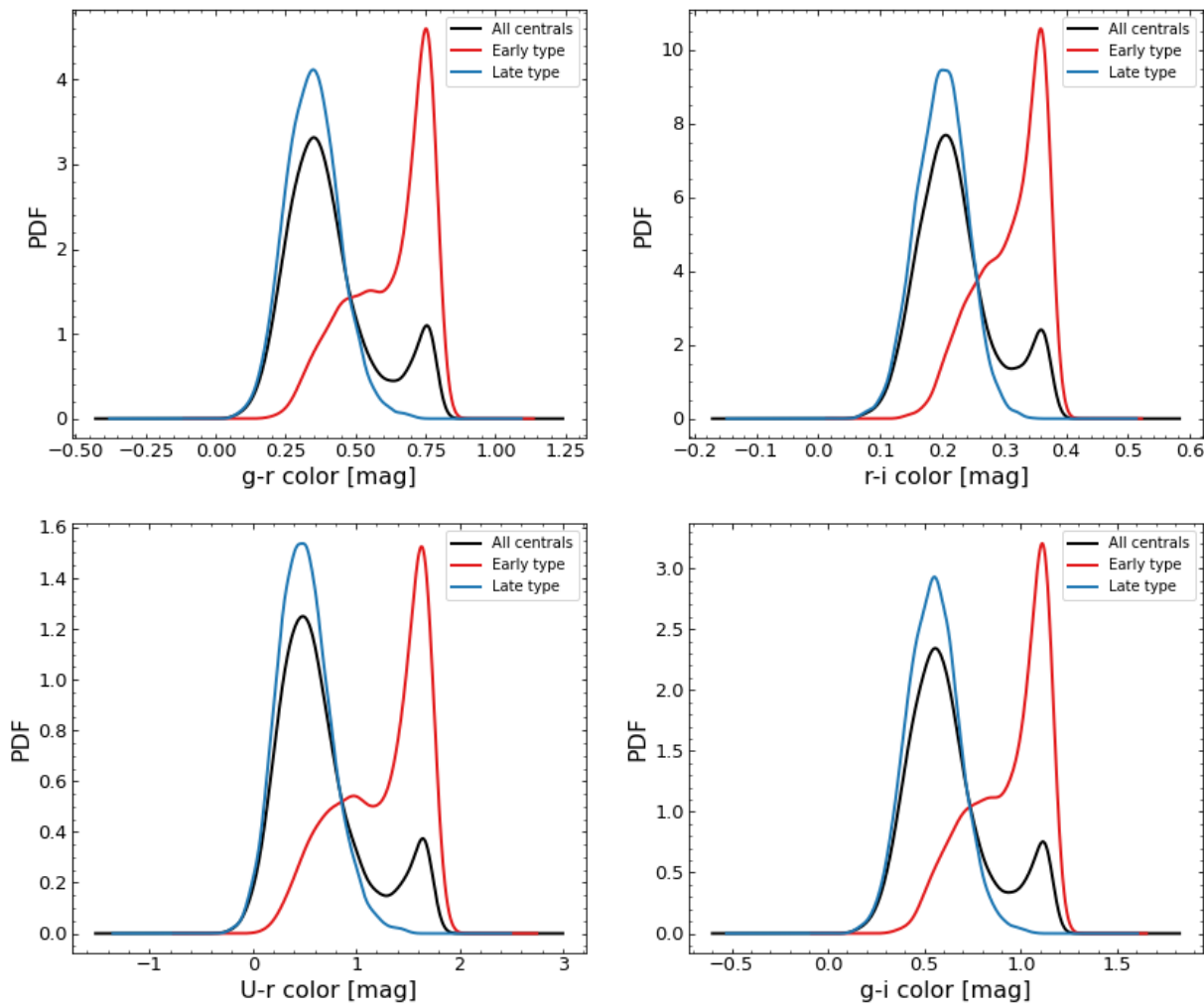


Figure 13

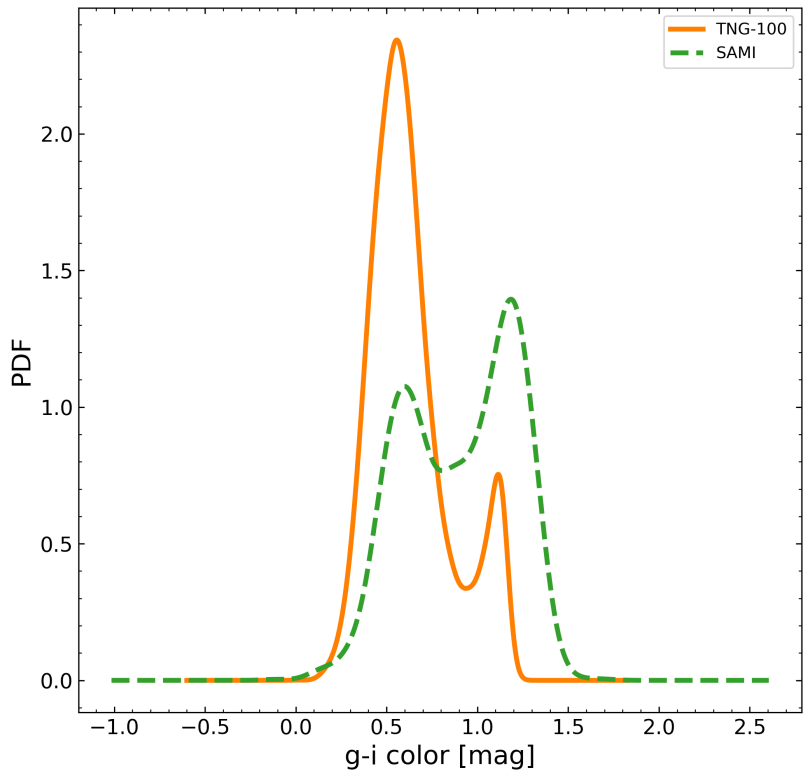


Figure 14

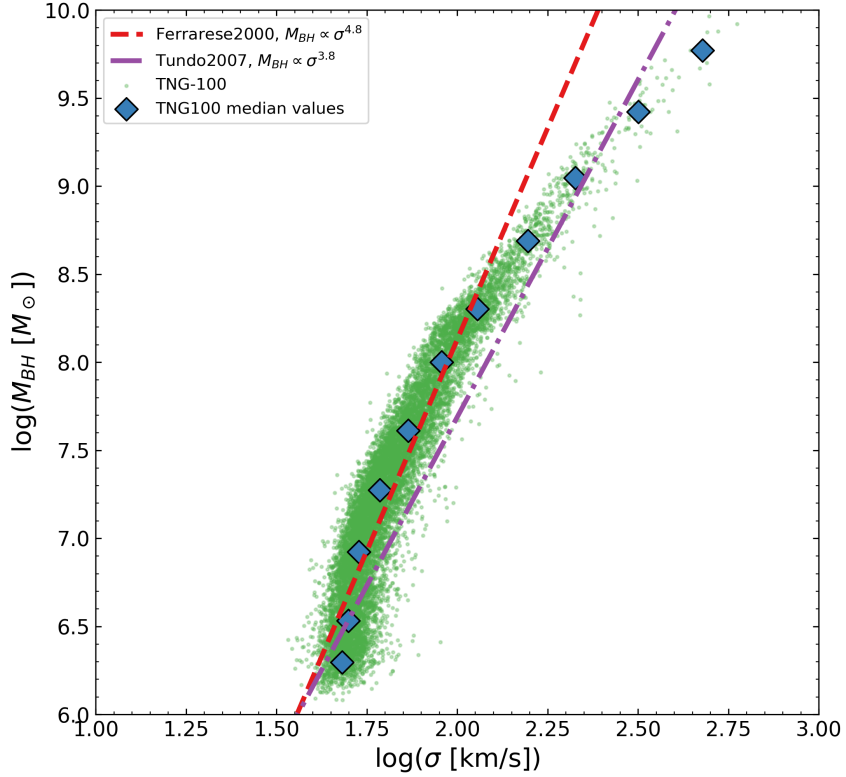


Figure 15

## 4.5 SMBH relations

In Figure 15 the SMBH-mass and velocity dispersion for TNG100 is shown, along with the best fit functions from Ferrarese et al. 2000 and Tundo et al. 2007.

## 5 Conclusions

## References

- [1] P. A. R. Ade et al. “Planck2015 results”. In: *Astronomy & Astrophysics* 594 (Sept. 2016), A13. ISSN: 1432-0746. DOI: 10.1051/0004-6361/201525830. URL: <http://dx.doi.org/10.1051/0004-6361/201525830>.
- [2] Peter S. Behroozi et al. “The Average Star Formation Histories of Galaxies in Dark Matter Halos from  $z = 0\text{--}8$ ”. In: *The Astrophysical Journal* 770.1, 57 (June 2013), p. 57. DOI: 10.1088/0004-637X/770/1/57. arXiv: 1207.6105 [astro-ph.CO].
- [3] J. V. Bloom et al. “The SAMI Galaxy Survey: the low-redshift stellar mass Tully–Fisher relation”. In: *Monthly Notices of the Royal Astronomical Society* 472.2 (July 2017), pp. 1809–1824. ISSN: 1365-2966. DOI: 10.1093/mnras/stx1701. URL: <http://dx.doi.org/10.1093/mnras/stx1701>.
- [4] Antonio Boveia et al. “Dark Matter Searches at Colliders”. In: *Annual Review of Nuclear and Particle Science* 68.1 (Oct. 2018), pp. 429–459. ISSN: 1545-4134. DOI: 10.1146/annurev-nucl-101917-021008. URL: <http://dx.doi.org/10.1146/annurev-nucl-101917-021008>.
- [5] Christopher J. Conselice et al. “The evolution of galaxy number density at  $z < 8$  and its implications”. In: *The Astrophysical Journal* 830.2 (Oct. 2016), p. 83. ISSN: 1538-4357. DOI: 10.3847/0004-637X/830/2/83. URL: <http://dx.doi.org/10.3847/0004-637X/830/2/83>.
- [6] Darren J. Croton. “Damn You, Little  $h$ ! (Or, Real-World Applications of the Hubble Constant Using Observed and Simulated Data)”. In: *Publications of the Astronomical Society of Australia* 30 (2013). ISSN: 1448-6083. DOI: 10.1017/pasa.2013.31. URL: <http://dx.doi.org/10.1017/pasa.2013.31>.
- [7] S. Djorgovski et al. “Fundamental Properties of Elliptical Galaxies”. In: *The Astrophysical Journal* 313 (Feb. 1987), p. 59. DOI: 10.1086/164948.
- [8] S. M. Faber et al. “Velocity dispersions and mass-to-light ratios for elliptical galaxies.” In: *The Astrophysical Journal* 204 (Mar. 1976), pp. 668–683. DOI: 10.1086/154215.

- [9] Laura Ferrarese et al. “A Fundamental Relation between Supermassive Black Holes and Their Host Galaxies”. In: *The Astrophysical Journal* 539.1 (Aug. 2000), pp. L9–L12. ISSN: 0004-637X. DOI: 10.1086/312838. URL: <http://dx.doi.org/10.1086/312838>.
- [10] C. S. Frenk et al. “Nonlinear evolution of large-scale structure in the universe”. In: *The Astrophysical Journal* 271 (Aug. 1983), pp. 417–430. DOI: 10.1086/161209.
- [11] Shy Genel et al. “The size evolution of star-forming and quenched galaxies in the IllustrisTNG simulation”. In: *Monthly Notices of the Royal Astronomical Society* 474.3 (Nov. 2017), pp. 3976–3996. ISSN: 1365-2966. DOI: 10.1093/mnras/stx3078. URL: <http://dx.doi.org/10.1093/mnras/stx3078>.
- [12] E. P. Hubble. “Extragalactic nebulae.” In: *The Astrophysical Journal* 64 (Dec. 1926), pp. 321–369. DOI: 10.1086/143018.
- [13] Lee S. Kelvin et al. “Galaxy And Mass Assembly (GAMA): Structural Investigation of Galaxies via Model Analysis”. In: *Monthly Notices of the Royal Astronomical Society* 421.2 (Mar. 2012), pp. 1007–1039. ISSN: 0035-8711. DOI: 10.1111/j.1365-2966.2012.20355.x. URL: <http://dx.doi.org/10.1111/j.1365-2966.2012.20355.x>.
- [14] Houjun Mo, Frank van den Bosch, et al. *Galaxy Formation and Evolution*. Cambridge University Press, 2010. DOI: 10.1017/CBO9780511807244.
- [15] Houjun Mo, Frank C. van den Bosch, et al. *Galaxy Formation and Evolution*. 2010.
- [16] Benjamin P. Moster et al. “Galactic star formation and accretion histories from matching galaxies to dark matter haloes”. In: *Monthly Notices of the Royal Astronomical Society* 428.4 (Dec. 2012), pp. 3121–3138. ISSN: 1365-2966. DOI: 10.1093/mnras/sts261. URL: <http://dx.doi.org/10.1093/mnras/sts261>.
- [17] Julio F. Navarro et al. “The Structure of Cold Dark Matter Halos”. In: *The Astrophysical Journal* 462 (May 1996), p. 563. DOI: 10.1086/177173. arXiv: [astro-ph/9508025 \[astro-ph\]](#).
- [18] William H. Press et al. “Formation of Galaxies and Clusters of Galaxies by Self-Similar Gravitational Condensation”. In: *The Astrophysical Journal* 187 (Feb. 1974), pp. 425–438. DOI: 10.1086/152650.
- [19] Jesse van de Sande et al. “The SAMI Galaxy Survey: comparing 3D spectroscopic observations with galaxies from cosmological hydrodynamical simulations”. In: *Monthly Notices of the Royal Astronomical Society* 469.3 (Oct. 2017), pp. 2873–2892. DOI: 10.1093/mnras/stw2902. URL: <http://dx.doi.org/10.1093/mnras/stw2902>.

- Society* 484.1 (Dec. 2018), pp. 869–891. ISSN: 1365-2966. DOI: 10.1093/mnras/sty3506. URL: <http://dx.doi.org/10.1093/mnras/sty3506>.
- [20] P. Schechter. “An analytic expression for the luminosity function for galaxies.” In: *The Astrophysical Journal* 203 (Jan. 1976), pp. 297–306. DOI: 10.1086/154079.
- [21] Nicholas Scott et al. “The SAMI Galaxy Survey: Data Release Two with absorption-line physics value-added products”. In: *Monthly Notices of the Royal Astronomical Society* 481.2 (Aug. 2018), pp. 2299–2319. ISSN: 1365-2966. DOI: 10.1093/mnras/sty2355. URL: <http://dx.doi.org/10.1093/mnras/sty2355>.
- [22] Jeremy Tinker et al. “Toward a Halo Mass Function for Precision Cosmology: The Limits of Universality”. In: *The Astrophysical Journal* 688.2 (Dec. 2008), pp. 709–728. DOI: 10.1086/591439. arXiv: 0803.2706 [astro-ph].
- [23] R. B. Tully et al. “Reprint of 1977A&A....54..661T. A new method of determining distance to galaxies.” In: *The Astrophysical Journal* 500 (Feb. 1977), pp. 105–117.
- [24] Elena Tundo et al. “On the Inconsistency between the Black Hole Mass Function Inferred from  $M_{\odot} - \sigma$  and  $M_{\odot} - L$  Correlations”. In: *The Astrophysical Journal* 663.1 (July 2007), pp. 53–60. ISSN: 1538-4357. DOI: 10.1086/518225. URL: <http://dx.doi.org/10.1086/518225>.
- [25] Rainer Weinberger et al. “Simulating galaxy formation with black hole driven thermal and kinetic feedback”. In: *Monthly Notices of the Royal Astronomical Society* 465.3 (Nov. 2016), pp. 3291–3308. ISSN: 1365-2966. DOI: 10.1093/mnras/stw2944. URL: <http://dx.doi.org/10.1093/mnras/stw2944>.
- [26] Lorenzo Zanisi et al. “Galaxy sizes and the galaxy–halo connection – I. The remarkable tightness of the size distributions”. In: *Monthly Notices of the Royal Astronomical Society* 492.2 (Dec. 2019), pp. 1671–1690. ISSN: 1365-2966. DOI: 10.1093/mnras/stz3516. URL: <http://dx.doi.org/10.1093/mnras/stz3516>.
- [27] A V Zasov et al. “Dark matter in galaxies”. In: *Physics-Uspekhi* 60.1 (Jan. 2017), pp. 3–39. ISSN: 1468-4780. DOI: 10.3367/UFNe.2016.03.037751. URL: <http://dx.doi.org/10.3367/UFNe.2016.03.037751>.